Int J Thermophys (2007) 28:1893–1903
DOI 10.1007/s10765-007-0289-5

Realization of Low-Temperature Fixed Points of the ITS-90 at NMIJ/AIST

T. Nakano · O. Tamura · H. Sakurai

Published online: 17 October 2007

Abstract A new model of sealed cells with three thermometer wells for calibration of capsule-type thermometers at low-temperature fixed points of the International Temperature Scale of 1990 has been developed at the National Metrology Institute of Japan (NMIJ). The melting curves of Ar and O_2 obtained using the new cells show very flat plateaux and a linear temperature dependence as a function of the inverse liquid fraction ($1/F$) over the range $1/F = 1$ to $1/F = 20$ with a narrow melting curve width of 0.1 mK. The melting curves of Ne obtained with the new cell also show very flat plateaux and approximately linear temperature dependence versus $1/F$ and a narrow melting curve width of 0.1 mK, though with a slight concave structure at high $1/F$. The melting temperatures with the new cells agree with previous NMIJ sealed cells within 10 μK, which is similar to the reproducibility of the realization of the triple points at NMIJ. The source dependence of the triple-point temperature of Ne was investigated by filling two of the new cells from different sources of Ne. The difference in the realized triple point temperatures between the two sources is 0.031 mK, consistent with that estimated from isotope analysis. The uncertainties in the calibration of standard platinum resistance thermometers at the low-temperature fixed points are summarized. The uncertainty of the calibration at the triple point of e-H_2 has been reduced to about one-third of its value without the correction by making the isotopic correction on the basis of the technical annex for the ITS-90 in the *mise en pratique* for the definition of the kelvin.

Keywords Ar · e-H_2 · ITS-90 · Low-temperature fixed points · Ne · O_2 · Uncertainty

T. Nakano (✉) · O. Tamura · H. Sakurai
National Metrology Institute of Japan (NMIJ), AIST, Central 3 1-1-1, Umezono, Tsukuba, Ibaraki 305-8563, Japan
e-mail: tnt@ni.aist.go.jp

1 Introduction

At the National Metrology Institute of Japan (NMIJ), new-generation sealed cells have been developed [1,2] to realize the triple points of argon (Ar), oxygen (O_2), neon (Ne), and equilibrium hydrogen (e-H_2), all of which are defining fixed points of the International Temperature Scale of 1990 (ITS-90) [3]. These low-temperature fixed points are used to calibrate standard platinum resistance thermometers, and the last two fixed points are also used to calibrate interpolating gas thermometers. Since a quick return to thermal equilibrium following a heat pulse is advantageous for the realization of these low-temperature fixed points at the highest level of accuracy by adiabatic calorimetry, the new-generation sealed cells employ oxygen-free high-conductivity (OFHC) copper for its high thermal diffusivity at low temperature. As reported earlier, the cells enable us to obtain very flat melting-curve plateaux for these low-temperature fixed points [1,2].

However, calibrations of thermometers using the cells involve some disadvantages: calibration of several thermometers is time consuming, because the new-generation sealed cells have only a single thermometer well. (Hereafter, the new-generation sealed cells having single thermometer wells are referred to as single-well cells.) Furthermore, if instability is observed during the calibration of a thermometer using a single-well cell, it is difficult to determine whether its origin is the cell or the thermometer.

As reported in [4–9], these drawbacks can be resolved by using cells with multiple thermometer wells. We have designed a new model of sealed cell for calibrating three capsule-type standard thermometers simultaneously. (Hereafter, the new model of sealed cell is called a multi-well cell.) To keep the thermal performance of the multi-well cell similar to that of the single-well cell, the multi-well cell was based on the single-well design. For the present study, the triple points of Ar, O_2, and Ne were realized calorimetrically [1,10] using the new multi-well cells; we confirmed that the triple-point temperatures obtained with the multi-well cells agree within 10 μK at the triple points of Ar, O_2, and Ne with those of the single-well cells.

In this report, we first describe the realizations of the triple points of Ar, O_2, and Ne. Then, we explore the source dependence of the triple-point temperature of Ne by using two multi-well cells filled from different sources of Ne. The estimated difference in the realized triple-point temperatures between the two sources is 0.031 mK, consistent with that estimated from isotopic analysis [11].

Finally, we summarize the uncertainties in the calibration of standard platinum resistance thermometers at the low-temperature fixed points at NMIJ. We also describe the reduction in the uncertainty of the triple point of e-H_2 by correcting the triple-point temperature for the isotopic composition as described in the technical annex for the ITS-90 in the *mise en pratique* for the definition of the kelvin [12].

2 Experimental

Figure 1 is a schematic illustration of the multi-well cell, whose design was based on our single-well cell [1]. To quickly attain thermal equilibrium between the thermometers and the phase-transforming substance, the multi-well cell is constructed from

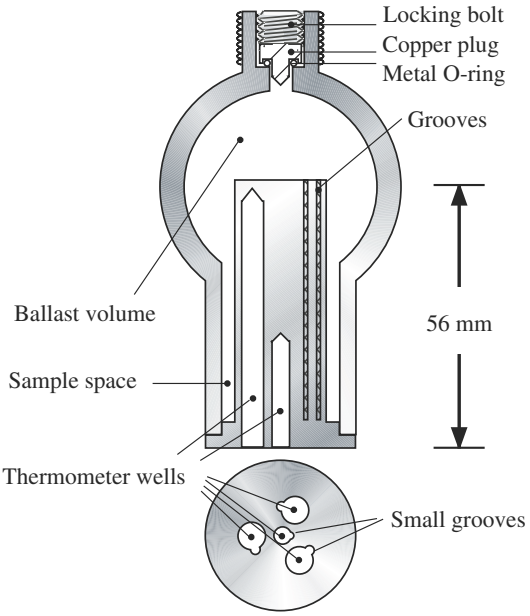

Fig. 1 Multi-well model of new-generation NMIJ sealed cell

oxygen-free high conductivity copper. The shape of the multi-well cell and its inner volume are almost the same as the single-well cell [1]. The upper part of the multi-well cell is a spherical vessel, primarily for pressure ballast, and the lower part is a cylindrical block which has three re-entrant wells for capsule-type standard platinum resistance thermometers or rhodium–iron resistance thermometers. The middle of the copper block also contains a re-entrant well for a thermometer for temperature control. Each thermometer well has a small groove for easy evacuation of residual gas from the space around the thermometer prior to the cooling of the cells to realize the low-temperature fixed points. The sealing device and the filling system for the multi-well cell are the same as those used for the single-well model [1].

Table 1 summarizes the samples used to realize the low-temperature fixed points at NMIJ, along with the impurity analyses provided by the suppliers. Table 2 provides an overview of the sealed cells of NMIJ. In the present study, we used the single-well cells [2] NMIJ A-3, NMIJ O-1, and NMIJ Ne-1, and the multi-well cells NMIJ A-4, NMIJ O-2, NMIJ Ne-2, and NMIJ Ne-5 to realize the triple points of Ar, O_2, and Ne.

To realize the low-temperature fixed points, we use a calorimeter on the basis of a two-stage Gifford-McMahon refrigerator [1,10]. The temperature of the adiabatic shield surrounding the sealed cell [1,10] is always controlled so as to reduce the spurious heat flux to less than 10 μW at the triple point of Ar and 5 μW at the triple points of O_2 and Ne, as estimated from the temperature drift of the cell below and above the triple point for all runs of each cell [10].

The heat for the calorimetry was calculated from the electric power applied to the resistance heater wound around the cell and the period of heating [1,2,10]. Since

Table 1 List of materials for realization of low-temperature fixed points at NMIJ and their impurity elements

Impurity elements as analyzed by suppliers										
Material	Gas purity	Gas source	O_2 (ppm)	N_2 (ppm)	H_2 (ppm)	CO (ppm)	CO_2 (ppm)	C_mH_n (ppm)	Ar (ppm)	He (ppm)
Ar	>6N[a]	NSC[b]	<0.02	<0.1	<0.05	<0.01	<0.01	<0.01	–	–
O_2	>6N5	NSC[b]	–	<0.2	–	<0.02	<0.02	<0.02	<0.05	–
Ne	>5N	Iceblick[c]	<0.5	<2.0	<1	<0.5	<0.5	<0.5	–	<8.0
Ne	>5N	Air water[d]	<0.5	<0.5	<0.3	<0.2	<0.05	<0.2	–	<5.0
H_2[e]	>7N	NSC[b]	<0.02	<0.05	–	<0.01	<0.01	<0.01	–	–

[a] 6N means 99.9999%
[b] Nippon Sanso Corp.
[c] Iceblick Ltd.
[d] Air Water Inc.
[e] D/H ratio; 27.2 (0.2) μmol D/ mol H [1]

Table 2 List of sealed cells used in this study.

Fixed point	Serial number	Cell model	Sample content (mmol)	τ ($F = 90\%$)[b] (min)
Ar	NMIJ A-3	Single-well [2]	66	0.7
Ar	NMIJ A-4	Multi-well	85	0.7
O_2	NMIJ O-1	Single-well [2]	72	0.6
O_2	NMIJ O-2	Multi-well	64	0.4
Ne	NMIJ Ne-1	Single-well [2]	79	0.2
Ne	NMIJ Ne-2	Multi-well	70	0.2
Ne	NMIJ Ne-5	Multi-well	61	0.2
e-H_2	NMIJ H-5[a]	Single-well [2]	90	0.1

[a] NMIJ H-5 cell contains 0.015 g of FeO(OH) as a catalyst to ensure the ortho-para equilibration of molecular hydrogen [1]
[b] τ and F are the thermal recovery time constant and the melted fraction of the sample in each sealed cell, respectively

both models of cells are of the same material and design, it is expected that they will have identical thermal performance. As shown in Table 2, the thermal recovery time constants, τ, after the heating pulses are less than 1 min at a melted fraction of 90% for both models of cells and show very close agreement at each fixed point. This is consistent with our expectation.

Platinum resistance thermometers were used for the measurements of the triple points of Ar, O_2, and Ne. Rhodium–iron resistance thermometers were also used for the measurements of the triple point of Ne. These resistances were measured by means of an automatic direct current comparator bridge. Excitation currents, I, for the measurement of platinum resistance thermometers were $I = 0.5$ mA or $I = 1$ mA

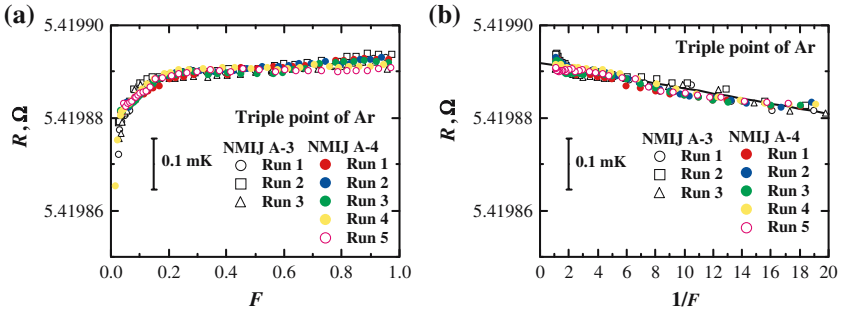

Fig. 2 Melting curves for Ar cells, NMIJ A-3 (single-well model) and NMIJ A-4 (multi-well model), (**a**) plotted against the melted fraction, F, and (**b**) plotted against $1/F$. A platinum resistance thermometer was used for the measurements

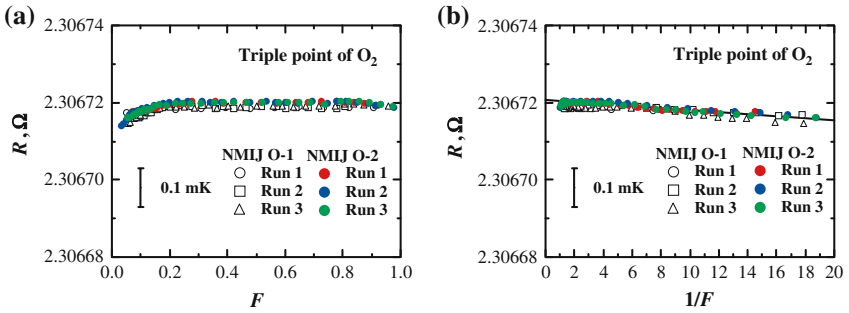

Fig. 3 Melting curves for O_2 cells, NMIJ O-1 (single-well model) and NMIJ O-2 (multi-well model), (**a**) plotted against the melted fraction, F, and (**b**) plotted against $1/F$. A platinum resistance thermometer was used for the measurements

at the triple points of Ar and O_2, and $I = 2$ mA at the triple point of Ne. We used $I = 0.5$ mA for the measurement of rhodium–iron resistance thermometers at the triple point of Ne. The results reported here are given for zero thermometer current obtained by extrapolating the observation made at I and that made at $\sqrt{2}I$ to correct for self-heating effects.

3 Results and Discussion

3.1 Realization of the Triple Points of Ar and O_2

Figure 2a and b shows the melting curves at the triple point of Ar, and Fig. 3a and b shows the melting curves at the triple point of O_2. These melting curves were obtained after thermal treatment to suppress the influence on the melting curves from the portion of solid at low-melted fraction, F (high $1/F$) [2]. The thermal treatment also reduces the influence of crystal quality as reported in [13,14].

The typical thermal treatment proceeds as follows: (1) the sample is completely solidified; (2) about half of the solid is melted, and the half-melted sample is kept for

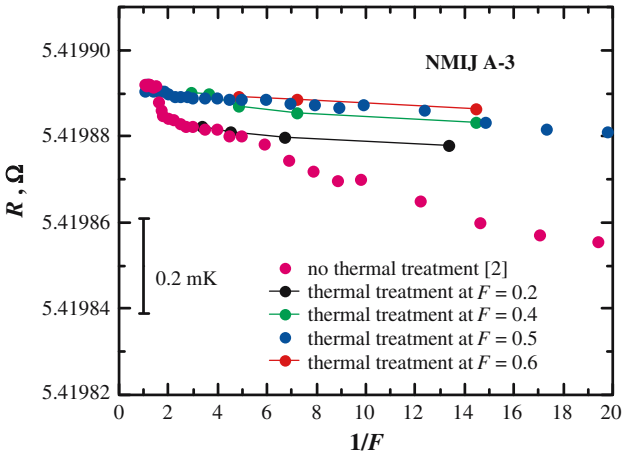

Fig. 4 Example of the effect of thermal treatment on the melting curves for NMIJ A-3. The melting curve obtained without the thermal treatment was reported in [2]

about 2 h in an adiabatic environment; then (3) the sample is completely re-solidified [2]. To confirm the optimal thermal treatment, we observed the melting curves after partially melting different fractions F for the process (2) using the NMIJ A-3 cell. As shown in Fig. 4, partial melting to $F = 0.5$ is efficient in suppressing the influence of the first-melted solid portion. The optimal procedure for the thermal treatment of a particular sample depends on the conditions of solidification, the cell materials, the heat transfer conditions, the sample purity, and other factors. To obtain more reliable melting curves, we have established the optimum procedure for each cell.

As shown in the figures, the melting curves obtained with both types of cells show very flat plateaux over a wide melted fraction, $F(F > 0.2)$, a linear dependence on $1/F$ in the range from $1/F = 1$ to $1/F = 20$, and a narrow width of the melting curve—within 0.1 mK. Furthermore, the melting curves obtained by both models of cells show very close agreement over a wide range of the melted fraction for the triple points of Ar and O_2. If the melting temperature is obtained by using the melting curves at $F > 0.5$ on the basis of the recommendation of Working Group 1 (WG1) of the Consultative Committee for Thermometry (CCT) [15], the melting temperatures agree within 10 μK, which is similar to the reproducibility of the realizations of the triple points of Ar and O_2 using each model of cell at NMIJ.

3.2 Realization of the Triple-Point Temperature of Ne

Figure 5a and b shows the melting curves at the triple point of Ne, which are obtained after thermal treatment [2]. Both melting curves show very flat plateaux at $F > 0.2$. On the other hand, melting curves obtained using the NMIJ Ne-1 cell deviate from those obtained using NMIJ Ne-2 for $F < 0.2$. The difference between the melting curves is also clearly observed when plotted against $1/F$ (Fig. 5b). The origin of the difference is

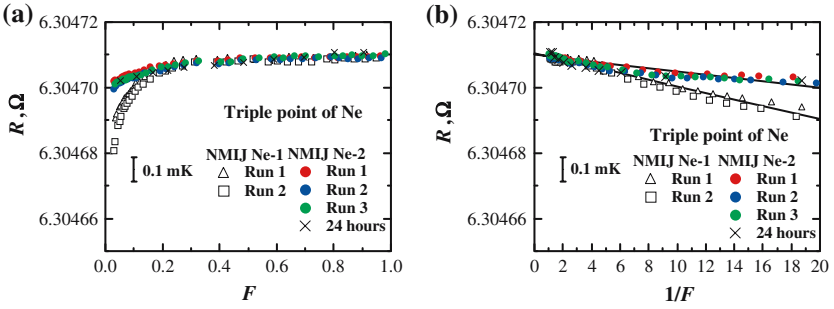

Fig. 5 Melting curves for Ne cells, NMIJ Ne-1 (single-well model) and NMIJ Ne-2 (multi-well model), (**a**) plotted against the melted fraction, F, and (**b**) plotted against $1/F$. A rhodium-iron resistance thermometer was used for the measurements

unclear from this study alone, but may be caused by impurities accidentally introduced into the NMIJ Ne-1 cell.

The melting curves plotted against $1/F$ show an approximately linear dependence for both cells, although they may have a slightly concave structure at $1/F > 10$. This may be characteristic of the mixture of three Ne isotopes, or it may be due to the long decay following heat pulses as reported in [14,16]. For the realization of the triple point of Ne, a long decay time (over 5 h) to reach thermal equilibrium has been observed after heat pulses at $1/F > 10$ and this has been attributed to the mixture of three Ne isotopes [14,16]. As shown in Fig. 6, we also observed a long decay. In this study, we took temperature values for each melted fraction when the decay rate was much less than $-3\mu\mathrm{K}\cdot\mathrm{h}^{-1}$. To check the effect of the long decay on the melting curves, we also took the temperature values 24 h following heat pulses at several melted fractions for NMIJ Ne-2, as shown in Fig. 5a and b. The temperature values obtained on the basis of the decay rate as described above agree with those at 24 h following heat pulses within the repeatability of the melting curves for NMIJ Ne-2. Further investigations with widely different isotope content are needed to discuss the detailed structure of the melting curves of Ne at $1/F > 10$.

The flat parts of the melting curves plotted against F for both cells agree well. If the melting temperature is obtained on the basis of the recommendation of WG1 of the CCT [15] in the same manner as that for the triple points of Ar and O_2, they agree within 10 μK, which is the level of reproducibility for the realization of the triple point of Ne using each cell at NMIJ. This indicates that the triple-point temperatures realized using the same Ne source agree very well, although a difference is seen between the melting curves of different cells.

Figure 7 shows the melting curves obtained using cells NMIJ Ne-2 and NMIJ Ne-5 to investigate the source dependence of the triple-point temperature of Ne using two different sources of Ne. The vertical axis is the difference between the measured temperature, T_e, and the triple point temperature for NMIJ Ne-5, T_{FP} (Ne-5), estimated in the same manner as for NMIJ Ne-2.

The melting curves for NMIJ Ne-5 are similar in shape to those for NMIJ Ne-2. However, a difference is seen between the triple-point temperatures for NMIJ Ne-2

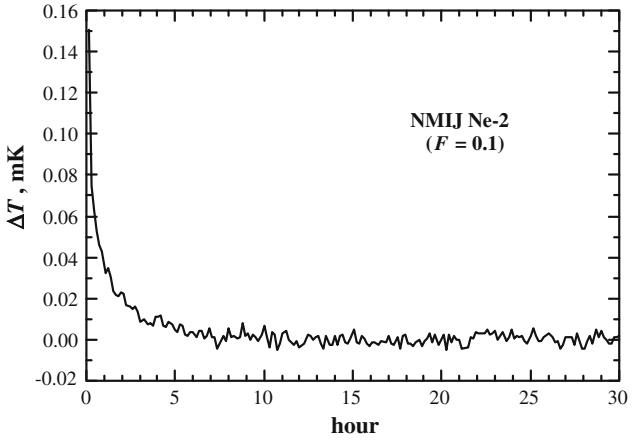

Fig. 6 Response curve of temperature of NMIJ Ne-2 cell after a heat pulse from about $F = 0.05$ to about $F = 0.1$

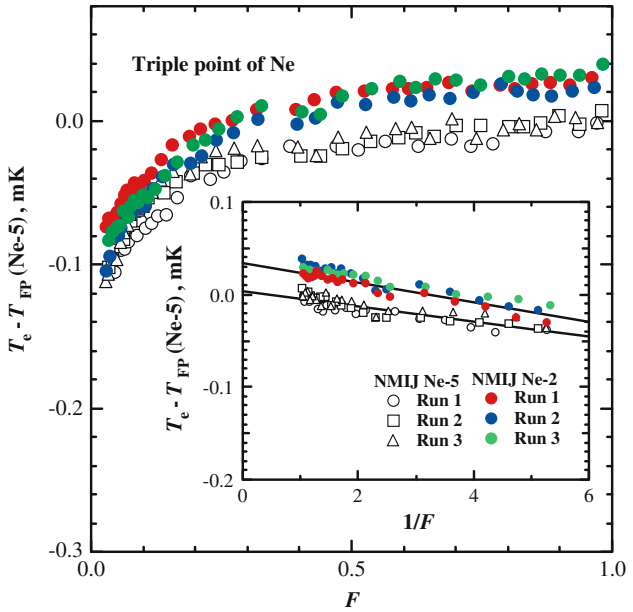

Fig. 7 Comparison of the melting curves using different sources of Ne plotted against the melted fraction, F. The inset shows enlarged melting curves plotted against $1/F$. The vertical axis plots the difference between the measured temperature, T_e, and the melting temperature for NMIJ Ne-5 cells, T_{FP}(Ne-5)

and NMIJ Ne-5. The difference is estimated to be 0.031 mK, which is consistent with that estimated from isotopic analysis of the two sources [11]. Detailed results of the isotopic analysis are presented elsewhere in these proceedings [11].

Table 3 Uncertainty budgets for the calibration of a capsule-type platinum resistance thermometer at the low-temperature fixed points using NMIJ sealed cells

Fixed point	e-H_2[a]	Ne	O_2	Ar	Hg[b]
Uncertainty components (mK)					
Realization					
Chemical impurities and isotopes	0.02 (0.2)[c]	0.14	0.009	0.022	0.057
Spin equilibrium and catalysts	0.041				
Hydrostatic effect	0.005	0.02	0.02	0.04	0.007
Thermal equilibrium	0.012	0.006	0.008	0.017	0.04
Reproducibility	0.019	0.01	0.01	0.01	0.012
Determination of FP value	0.008	0.010	0.011	0.007	0.030
Measurement					
Bridge accuracy	0.041	0.002	0.001	0.003	0.011
Standard resistor	0.002	0.003	0.009	0.019	0.015
Self heating correction	0.008	0.007	0.004	0.006	0.005
Propagation from H_2O TP	0.001	0.001	0.015	0.036	0.14
Standard combined uncertainty (mK)	0.065 (0.21)[c]	0.14	0.033	0.065	0.16

[a] Realization of the triple point of e-H_2 was reported previously [1,2,17]. Uncertainty component due to reproducibility for e-H_2 is estimated from data using standard platinum resistance thermometers as reported in [17]
[b] Realization of the triple point of Hg will be reported elsewhere
[c] Uncertainty in the case without isotopic correction [18]

3.3 Uncertainties in the Realization of Low-Temperature Fixed Points at NMIJ

Table 3 shows the present uncertainty budget for calibrating capsule-type standard platinum resistance thermometers at the low-temperature fixed points. We are currently taking part in a key comparison of capsule-type standard platinum resistance thermometers (CCT-K2.5) on the basis of these estimates. The uncertainty component for chemical impurities has been estimated using the overall maximum estimate (OME), ΔT_{OME}, recommended by Working Group 1 of the CCT, except for those impurities whose effect on the fixed-point temperature are known [15]. For impurities whose effects are known, the maximum shift of the melting temperature is calculated by summing the individual effects based on the known sensitivity coefficients [19–21] and the impurity concentrations from Table 1. This shift is then added to ΔT_{OME} to estimate the overall effect of impurities in what might be described as a modified-OME analysis.

In Table 3, the thermal equilibrium component is dominated by the so-called static temperature error estimated from the thermal resistance, R_{cs} [13,19]. The typical thermal resistances at $F = 90\%$ are 4, 1, 2, and $3\,\mathrm{K{\cdot}W^{-1}}$ for the H_2, Ne, O_2, and Ar cells, respectively. As mentioned above, the temperature of the adiabatic shield is controlled to suppress spurious heat flux to less than 10 μW at the triple point of Ar

and 5 μW at the triple points of O_2, Ne, and H_2, as estimated from the temperature drift of the cell below and above the triple point for all runs of each cell [10]. Therefore, we estimate the uncertainty from the static temperature error on the assumption that it is described by a symmetric, rectangular, a priori probability distribution.

Table 3 also shows the uncertainties for e-H_2 both with and without the isotopic correction based on the technical annex for the ITS-90 in the *mise en pratique* for the definition of the kelvin [12]. Without the isotopic correction, the combined uncertainty is dominated by the variability of the isotopic concentration of commercially available hydrogen, the standard uncertainty of which is 0.2 mK (type B evaluation) [13,18]. By applying the isotopic correction, we eliminate the large uncertainty caused by variability of the isotope concentration of hydrogen. The magnitude of the isotopic correction for the realized triple-point temperature of e-H_2 has been estimated using the equation [12,18] $\Delta T = k_D(x - x_o)$, where k_D is the triple-point temperature dependence on the deuterium ratio (5.42 (20) μK per μmol D/mol H) given by Fellmuth et al. [13], x is the isotopic ratio of the actual sample, and x_o is the reference isotopic ratio (89.02 per μmol D/mol H) assigned to the triple point of e-H_2 (T_{90} (e-H_2 TP) = 13.8033 K). Since the isotopic concentration of our sample is 27.2 (2) μmol D/mol H, ΔT and its uncertainty are estimated to be -0.335 and 0.02 mK, respectively. Therefore, the standard combined uncertainty for the calibration at the triple point of e-H_2 is reduced to about one-third of that without the isotopic correction.

As seen in Table 3, the uncertainty component related to isotopic composition is one of the dominant factors in the combined uncertainty of the triple point of Ne. This is caused by variability in the distribution of Ne isotopes from commercial sources [11,22]. If the isotopic correction at the triple point of Ne can be handled in the same way as was done for the triple point of e-H_2, we expect that the standard uncertainty will be reduced to the same level as estimated for the triple point of e-H_2.

Acknowledgments The authors thank Dr. Shimazaki and Dr. Nakagawa for valuable discussions and useful suggestions.

References

1. T. Nakano, O. Tamura, H. Sakurai, in *Temperature: Its Measurement and Control in Science and Industry*, vol 7. Part 1, ed. by D. Ripple (AIP, New York, 2003), pp. 185–190
2. T. Nakano, O. Tamura, H. Sakurai, in *Proc. TEMPMEKO 2004, 9th Int. Symp. on Temperature and Thermal Measurements in Industry and Science*, ed. by D. Zvizdić, L.G. Bermanec, T. Veliki, T. Stašić, (FSB/LPM, Zagreb, Croatia, 2005), pp. 159–164
3. H. Preston-Thomas, Metrologia **27**, 3 (1990)
4. F. Pavese, D. Ferri, in *Temperature: Its Measurement and Control in Science and Industry*, vol 5, Part 1, ed. by J.F. Schooley (AIP, New York, 1982), pp. 217–227
5. D.I. Head, R.L. Rusby, J.E. Martin, *NPL Report QM116* (National Physical Laboratory, Teddington, 1995), pp. 1–21
6. W.L. Tew, in *Proc. TEMPMEKO '96, 6th Int. Symp. on Temperature and Thermal Measurements in Industry and Science*, ed. by P. Marcarino (Levrotto Bella, Torino, 1997), pp. 81–86
7. B. Fellmuth, P. Seifert, H. Rudloff, in *Proc. TEMPMEKO '96, 6th Int. Symp. on Temperature and Thermal Measurements in Industry and Science*, ed. by P. Marcarino (Levrotto Bella, Torino, 1997), pp. 93–98

8. Y. Hermirer, L. Pitre, C. Geneville, A. Verge, G. Bonnier, D.I. Head, B. Fellmuth, L. Wolber, A. Szmyrka-Grzebyk, L. Lipinski, M.J. de Groot, A. Peruzzi, in *Temperature: Its Measurement and Control in Science and Industry*, vol 7, Part 1, ed. by D. Ripple (AIP, New York, 2003), pp. 179–184
9. K.D. Hill, A.G. Steele, in *Proc. TEMPMEKO 2004, 9th Int. Symp. on Temperature and Thermal Measurements in Industry and Science*, ed. by D. Zvizdić, L. G. Bermanec, T. Veliki, T. Stašić (FSB/LPM, Zagreb, Croatia, 2005), pp. 295–300
10. T. Nakano, O. Tamura, H. Sakurai, T. SICE **38**, 947 (2002) [in Japanese]
11. F. Pavese, B. Fellmuth, K.D. Hill, D. Head, Y. Hermier, L. Lipinski, T. Nakano, A. Peruzzi, H. Sakurai, A. Szmyrka-Grzebyk, A.D. Steele, P.P.M. Steur, O. Tamura, W.L. Tew, S. Valkier, L. Wolber, Progress Toward the Determination of $T - x$ for Neon Isotopes and the Update of CCT-K2 Results for Ne and e-H_2, in *Proc. TEMPMEKO 2007* (to be published in Int. J. Thermophys.)
12. Technical annex for the ITS-90 in the *mise en pratique* for the definition of the kelvin, http://www.bipm.fr/en/committees/cc/cct/
13. B. Fellmuth, L. Wolber, Y. Hermier, F. Pavese, P.P.M. Steur, I. Peroni, A. Szmyrka-Grzebyk, L. Lipinski, W.L. Tew, T. Nakano, H. Sakurai, O. Tamura, D. Head, A.G. Steele, Metrologia **42**, 171 (2005)
14. L. Wolber, B. Fellmuth, Influence of the Freezing and Annealing Conditions on the Realization of Cryogenic Triple Points. in *Proc. TEMPMEKO 2007* (to be published in Int. J. Thermophys.)
15. B. Fellmuth, K.D. Hill, P. Bloembergen, M. de Groot, Y. Hermier, M. Matveyev, A. Pokhodun, D. Ripple, P.P.M. Steur, Comite Consultatif de Thermometrie, 23rd Session, *Document CCT/05–08_Rev* (2005) and references therein
16. H. Sakurai, T. SICE **35**, 144 (1999) [in Japanese]
17. H. Sakurai, T. SICE **34**, 1553 (1999) [in Japanese]
18. P.P.M. Steur, Y. Hermier, K.S. Gam, K.D. Hill, B. Fellmuth, A.I. Pokhodun, D.C. Ripple, Comite Consultatif de Thermometrie, 23rd Session, *Document CCT/05–06/Rev(2)* (2005)
19. F. Pavese, in *Temperature: Its Measurement and Control in Science and Industry*, vol 7, Part 1, ed. by D. Ripple (AIP, New York, 2003), pp. 167–172
20. F. Pavese, G. Molinar, *Modern Gas-Based Temperature and Pressure Measurements* (Plenum Press, New York, 1992), pp. 464–471
21. J. Ancsin, Metrologia **14**, 1 (1978)
22. F. Pavese, B. Fellmuth, D. Head, Y. Hermier, K. Hill, S. Valkiers, Anal. Chem. **77**, 5076 (2005)